Multiaxial fatigue property of type 316 stainless steel using hollow cylinder specimen under combined pull loading and inner pressure

Takahiro Morishita
Postdoctoral researcher, Department of Mechanical Engineering, College of Science & Engineering, Ritsumeikan University, Japan
morisita@gst.ritsumei.ac.jp

Yuta Takada
Graduate student, Graduate school of Science & Engineering, Ritsumeikan University, Japan
rm0048hf@ed.ritsumei.ac.jp

Takamoto Itoh
Professor, Department of Mechanical Engineering, College of Science & Engineering, Ritsumeikan University, Japan
itohtaka@fc.ritsumei.ac.jp

ABSTRACT. Stress controlled multiaxial fatigue test was carried out using a hollow cylinder specimen of type 316 stainless steel. A newly developed fatigue testing machine which can apply push-pull loading and reversed torsion loading and inner pressure to the hollow cylinder specimen was employed. 5 types of cyclic loading paths were employed by combining zero to pull axial and hoop stresses: a Pull (only axial stress), an Inner-pressure (only hoop stress), an Equi-biaxial (equi-biaxial stress by axial and hoop stresses), a Square-shape (trapezoidal waveforms of axial and hoop stresses with 90-degree phase difference) and a L-shape (alternately axial stress and hoop stress) loading paths. Since directions of principal stresses are fixed in all the tests, all of the loading paths are classified into 'proportional loading'. In the Pull, the Inner-pressure and the Equi-biaxial tests, fatigue lives can be correlated on a unique line by a maximum equivalent stress based on von Mises. On the other hand, fatigue lives in the Square-shape and the L-shape tests were reduced comparing with that in the other tests, which was caused by yielding of larger plastic deformation.

KEYWORDS. Multiaxial fatigue; Inner pressure; Type 316 stainless steel; Hollow cylinder specimen; Proportional loading.

Citation: Morishita, T., Takada, Y., Itoh, T., Multiaxial fatigue property of type 316 stainless steel using hollow cylinder specimen under combined pull loading and inner pressure, Frattura ed Integrità Strutturale, 41 (2017) 71-78.

Received: 28.02.2017
Accepted: 15.04.2017
Published: 01.07.2017

INTRODUCTION

Many mechanical structures undergo multiaxial loading by diverse force. The equivalent stress based on von Mises (Mises stress) is generally used in that design for structures under multiaxial loading. In recent literatures of multiaxial fatigue, it is reported that fatigue life evaluated by the Mises stress is overestimated [1-8] and the

magnitude depends on loading path [9-16]. In the multiaxial fatigue under non-proportional loading in which directions of principal stress and strain are changed in a cycle, it has been reported that fatigue lives are reduced accompanying with additional hardening which depends on both loading path and material [4-16]. In addition, Itoh et al. presented a strain parameter for life evaluation under non-proportional loading considering the intensity of non-proportionality and the material dependency [12, 14]. However, the common testing machines cannot perform those kinds of tests. Therefore, the small amount of data of fatigue tests with a wide range of stress ratios is mainly due to the fact. In fact, the most common testing machine for multiaxial fatigue can perform only the push-pull loading and the reverse torsion loading which limits the stress ratio range from −1 to 0. To perform fatigue tests under wider stress ratio range like an equi-biaxial loading path, the testing machine need to be installed an actuator for inner pressure.

In this study, load controlled the fatigue tests at room temperature were carried out by a special testing machine which was developed by the authors [17]. The testing machine is an electric servo controlled multiaxial fatigue testing machine, which can combine the push-pull and the reversed torsion loads and the cyclic inner pressure. 5 types loading paths, which are a combination of the axial stress by the push-pull loading and the hoop stress by inner pressure, are employed in this study. The effect of loading paths on fatigue lives was discussed from the fatigue tests and observation of specimen surface.

MULTIAXIAL FATIGUE TESTING MACHINE

Fig. 1 shows the shape and dimensions of the hollow cylinder specimen of which dimensions are 12 mm inner diameter, 14 mm outer diameter and 8.5 mm gauge part. When the test specimen is gripped on testing rods, a plug guiding oil for the inner pressure is attached each side of the specimen as shown in Fig. 1 (b). An oil for inner pressure is shielded by an O-ring and a double specialty backup ring which can withstand high pressure over 200 MPa.

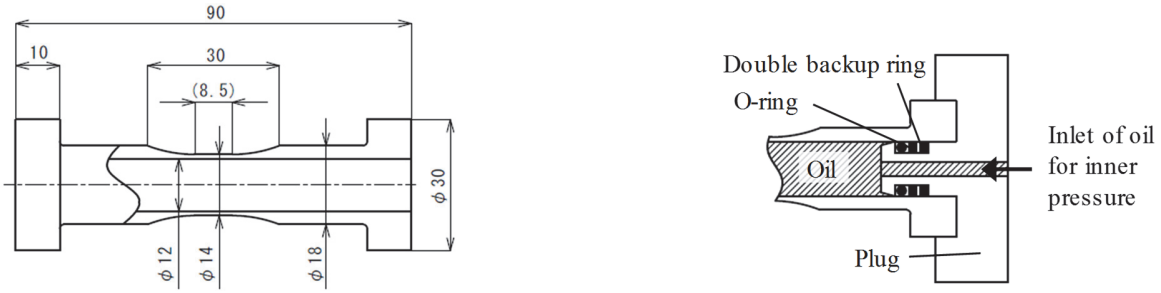

(a) Shape and dimensions of specimen (mm) (b) Schematic showing of inlet of oil for inner pressure

Figure 1: Hollow cylinder specimen.

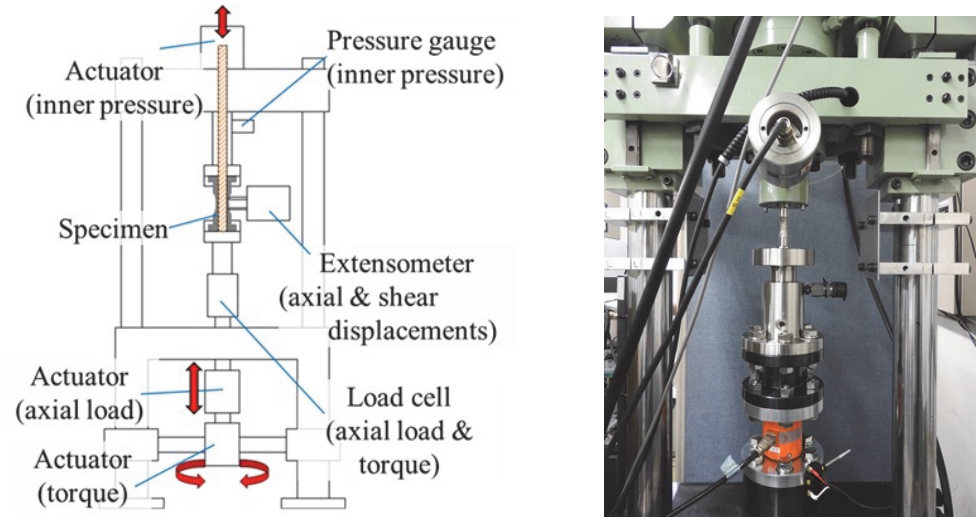

(a) Schematic view (b) Photo view

Figure 2: Multiaxial fatigue testing machine for push-pull and reversed torsion tests with inner pressure.

Fig. 2 (a) and (b) shows a schematic view and the picture of the multiaxial fatigue testing machine for the push-pull and the reversed torsion tests with the inner pressure. This testing machine is equipped with three actuators. The actuator in the upper side applies inner pressure and the two actuators in the lower side are used to apply the push-pull and the reversed torsion loading to the hollow cylinder specimen. The maximum pressure is applied to the inner surface of the specimen is 200 MPa. The maximum axial load for push-pull is ±50 kN, while the maximum torque for reversed torsion is ±250 N·m. By applying these loading paths, this testing machine can perform tests under wide range of multiaxial stress ratios.

A pressure gauge and the load cells are equipped to measure the inner pressure, the axial load and the torque. Fig. 3 shows two extensometers which measure axial and hoop displacements in the gauge part of the specimen. The extensometer for measurement of the axial displacement is attached directly onto the specimen as shown in Fig. 3 (a) and a gauge length is 7 mm. The extensometer for measurement of the hoop direction is attached by clamping the specimen thanks to a rubber band on the extremity of the device as shown in Fig. 3 (b).

(a) Axial displacement

(b) Hoop displacement

Figure 3: Extensometers to measure axial and hoop displacements.

MULTIAXIAL STRESS IN SPECIMEN

Fig. 4 (a) and (b) schematically show values of principal stresses in the specimen. The coordinate system of principal stresses is represented by axial, hoop and radial stresses due to absent shear stress. When the inner pressure is loaded, the axial stress σ_z, the hoop stress σ_θ and the radial stress σ_r are defined by the following equations,

$$\sigma_z = \frac{F}{\pi(r_O^2 - r_I^2)} + \frac{P r_I^2}{r_O^2 - r_I^2} \tag{1}$$

$$\sigma_\theta = \frac{P r_I^2}{r_O^2 - r_I^2}\left(1 + \frac{r_O^2}{r^2}\right) \tag{2}$$

$$\sigma_r = \frac{P r_I^2}{r_O^2 - r_I^2}\left(1 - \frac{r_O^2}{r^2}\right) \tag{3}$$

where F and P are the axial load and the inner pressure. r is an arbitrary radius into the specimen thickness direction, and r_O and r_I are the radii at the outer and the inner surfaces of the specimen, respectively: r_I=12 mm and r_O=14 mm. Equation of σ_z is added the second term due to additional stress by P independent of r. σ_θ and σ_r are dependent of r, and σ_θ takes the maximum value at r_O, while inversely σ_r decreases in negative value with increase of r.

The Mises stresses are different at the inner and the outer surfaces, which is described by;

$$\sigma_{eq}^{i} = \sqrt{\frac{1}{2}\left\{(\sigma_z - \sigma_\theta)^2 + (\sigma_\theta - \sigma_r)^2 + (\sigma_r - \sigma_z)^2\right\}} \tag{4}$$

where i indicates the position on the specimen (I: inner surface, M: middle between inner and outer surfaces, O: outer surface). For example, σ^{O}_{eq} is the Mises stress at the outside of specimen. σ^{M}_{eq} is that at the middle of specimen and σ^{I}_{eq} is that at the inside of specimen. σ_{eq} increases with decrease of r and takes the maximum one at the inner surface: i=I.

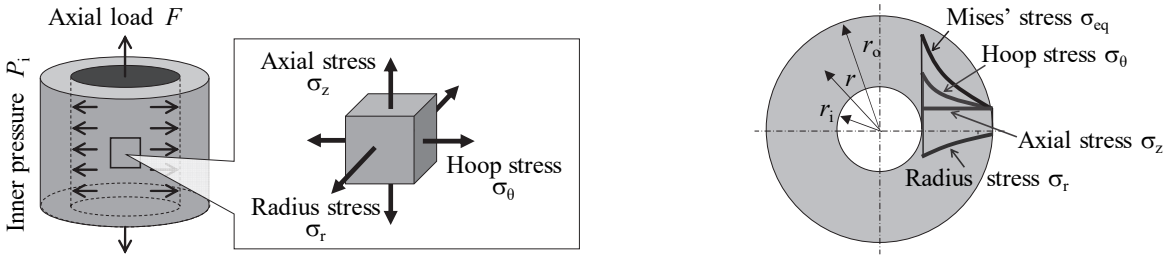

(a) Stress state in z-θ-r coodinates (b) Magnitudes of stresses on cross section

Figure 4: Directions and values of the principal stresses in the thickness direction of the specimen.

EXPERIMENTAL PROCEDURE

Type 316 stainless steel was employed as a testing material. The outer surface of gauge part was polished by 1μm alumina particles and finished as mirror-finished surfaces. The inner surface of the specimen was polished by emery papers up to #2000.

Load and pressure controlled fatigue tests were carried out at room temperature. Fig. 5 shows 5 types of loading waveforms and loading test paths: a Pull, an Inner-pressure, an Equi-biaxial, a Square-shape and a L-shape. The Pull is a cyclic pull loading in which only axial stress σ_z is applied. The Inner-pressure is a cyclic inner pressure test in which only hoop stress σ_θ is applied. These two loadings are classified as the uniaxial loading. The Equi-biaxial, the Square-shape and the L-shape are multiaxial loading tests in which combined cyclic pull loading and inner pressure are applied. In the Equi-biaxial test, axial stress σ_z and hoop stress σ_θ are applied simultaneously. In the Square-shape test, axial stress σ_z and hoop stress σ_θ are applied as trapezoidal waveforms with 90-degree phase difference so that the loading path is shown by a square shape in a σ_z-σ_θ coordinates. In the L-shape test, axial stress σ_z and hoop stress σ_θ are applied alternately so that the shape of loading path becomes the shape of the letter "L".

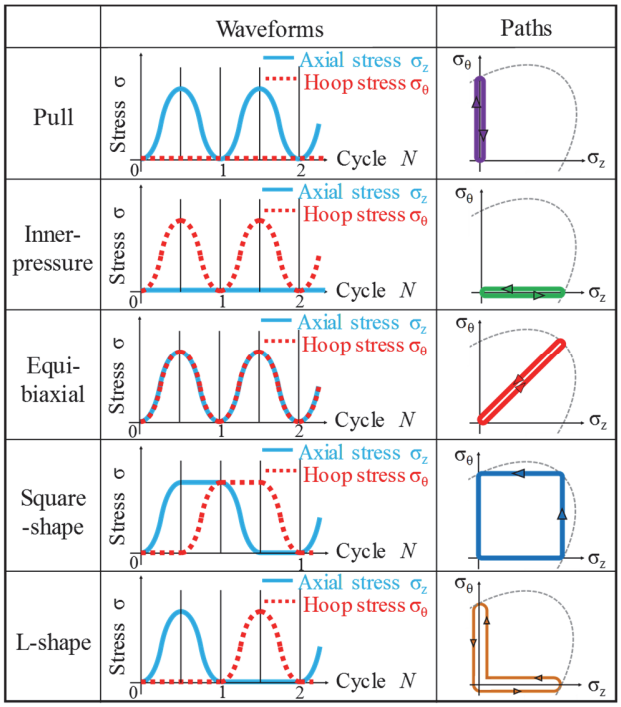

Figure 5: Loading waveforms and paths.

In the Equi-biaxial, the Square-shape and the L-shape tests, the axial stress and the hoop stress amplitudes are set to be the same as that on the outer surface. In the test condition, the maximum Mises stress at inside of the specimen $\sigma^{I}_{eq\ max}$ is 1.3 times larger than that at the outside of the specimen $\sigma^{M}_{eq\ max}$, in all the tests except the Pull test.
One cycle is counted when stress turns back origin in loading path. Therefore, a full path in the Pull, the Inner-pressure, the Equi-biaxial and the Square-shape tests one cycle, and that in the L-shape test is counted as two cycles. In the Pull test, constant inner pressure of 1 MPa was applied during test to unify definition of the N_f. Since the axial stress and the hoop stress generated due to the inner pressure of 1 MPa are 2.8 MPa and 6.5 MPa, the effect of the inner pressure is negligible in the testing load condition. Number of cycles to failure N_f is defined as the cycle at which the maximum inner pressure is reduced by the oil leak due to an initiation of through crack or rupture of the specimen.

TEST RESULTS

Fatigue life

Fig. 6 shows relationships between the maximum Mises stresses $\sigma^{i}_{eq\ max}$ at each measured position (i: O, M and I) and number of cycles to failure N_f. In the figures, N_f is reduced depend on loading path and cannot be evaluated uniquely by the maximum Mises stress.

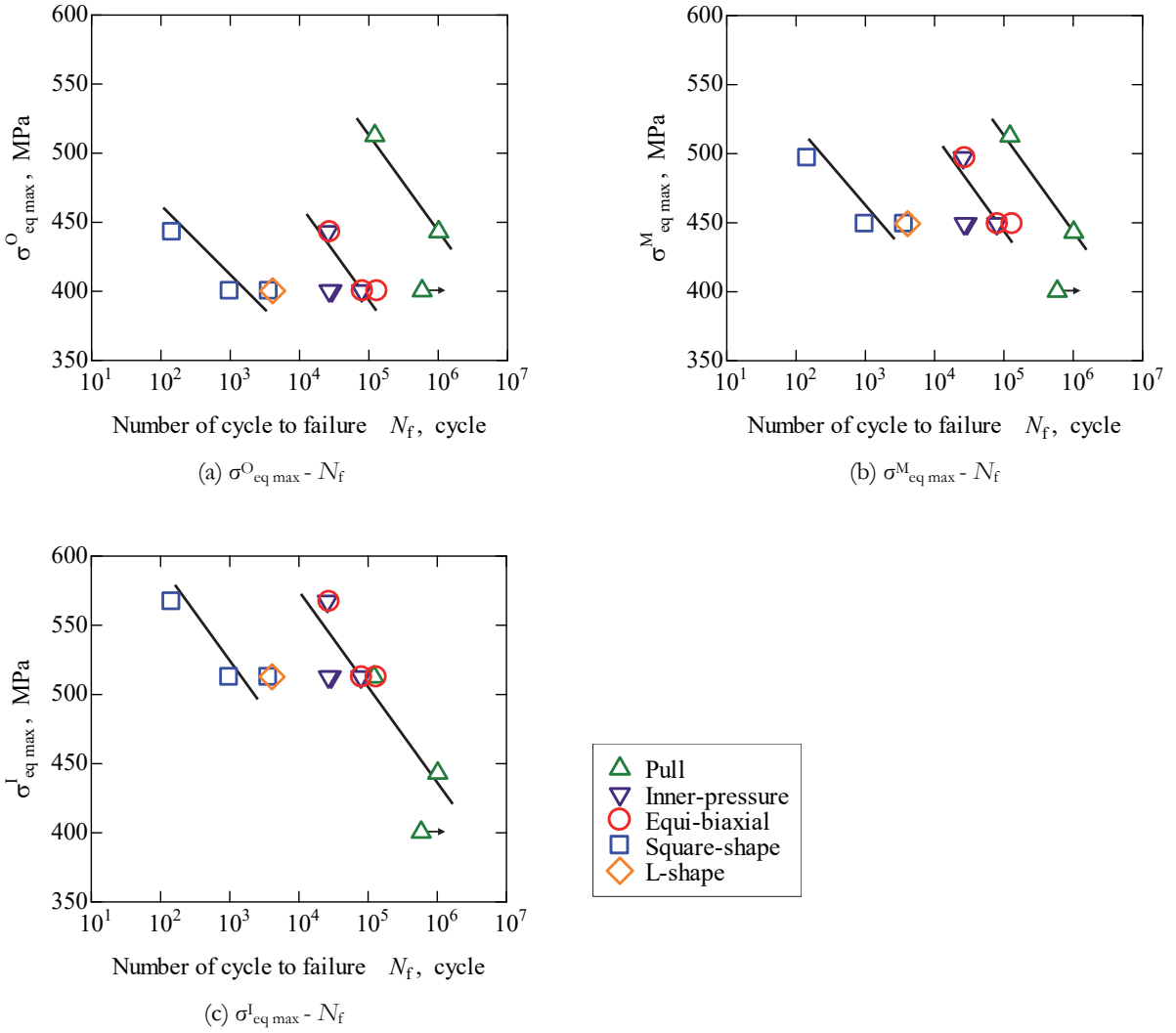

Figure 6: Relationship between maximum Mises stress and N_f at each measured position.

Fig. 6 (a) shows that N_f in the Inner-pressure and the Equi-biaxial tests are less than $0.3N_f$ in the Pull test. N_f in the Square-shape and the L-shape tests are much less and are overestimated by 3-4 orders in comparison with that in the Pull test. Although the reduction of N_f depending on loading path can be also seen in Fig. 6 (b), the overestimations of N_f are improved because the maximum Mises stresses $\sigma^{i}_{eq\ max}$ in all the tests except the Pull test increases by 0.1 defined as Eq.(4). In Fig. 6 (c), the overestimations become much less and N_f in the Pull, the Inner-pressure and the Equi-biaxial tests can be evaluated on a unique line by $\sigma^{I}_{eq\ max}$. The Pull and the Inner-pressure tests are equivalent and correspond to the uniaxial loading condition when the specimen geometry is ignored. In addition, crack initiations occurred from the inside of the specimen where σ_{eq} takes the maximum value. They suggest that $\sigma^{I}_{eq\ max}$ is the most suitable parameter to evaluate N_f. On the other hand, N_f in the Square-shape and the L-shape tests are still overestimated.

Fig. 7 shows Mohr's circle on each path, A, B and C, indicated in σ_θ-σ_z diagram and the maximum principal shear stress planes. Each plane has conjugate one but description of that is omitted here to show the image of planes on which slip may occur easier. On the planes, positive or negative symbol, '+, −', is indicated to show the slip direction. In all the paths, A, B and C, they have two planes. One is the plane normal to σ_θ-σ_z plane (the specimen surface) and the other is the plane inclined to the specimen surface by 45 degrees in the paths A and B. On the other hand, both the planes inclined to the specimen surface by 45 degrees exist in the path C. Therefore, the Pull and the Inner-pressure tests have experience of '+' and '−', respectively and the Equ-biaxial test '+' on the 45 degree-inclined the specimen surface. The L-shape test receives '+' and '−' alternatively which correspond to the fully reversed cyclic loading. The Square-shape test has experience of all these conditions during a cycle. There also existence of planes on which stress amplitude is equivalent in directions rotated between the planes; they are omitted here, too. Change in the slip plane is schematically shown in Fig. 8. Readers can understand easily that there is much possibility of slip activation in the L-path and the Square-shape tests than other three tests.

In strain controlled tests under multiaxial non-proportional loading, additional hardening due to non-proportional loading resulted from increase in interaction of activate slip systems which is related to additional damage have been reported [12]. In this study, stress and strain levels are relative small in which elastic deformation is dominant and directions of principal stress and strain are fixed into z-, θ- and r-directions. Thus, no or small additional hardening might occur and exitances of large number of possible activate slip plane and the reversed loading may influence on deformation and life properties, which results in the reduction in N_f in the L-path and the Square-shape tests.

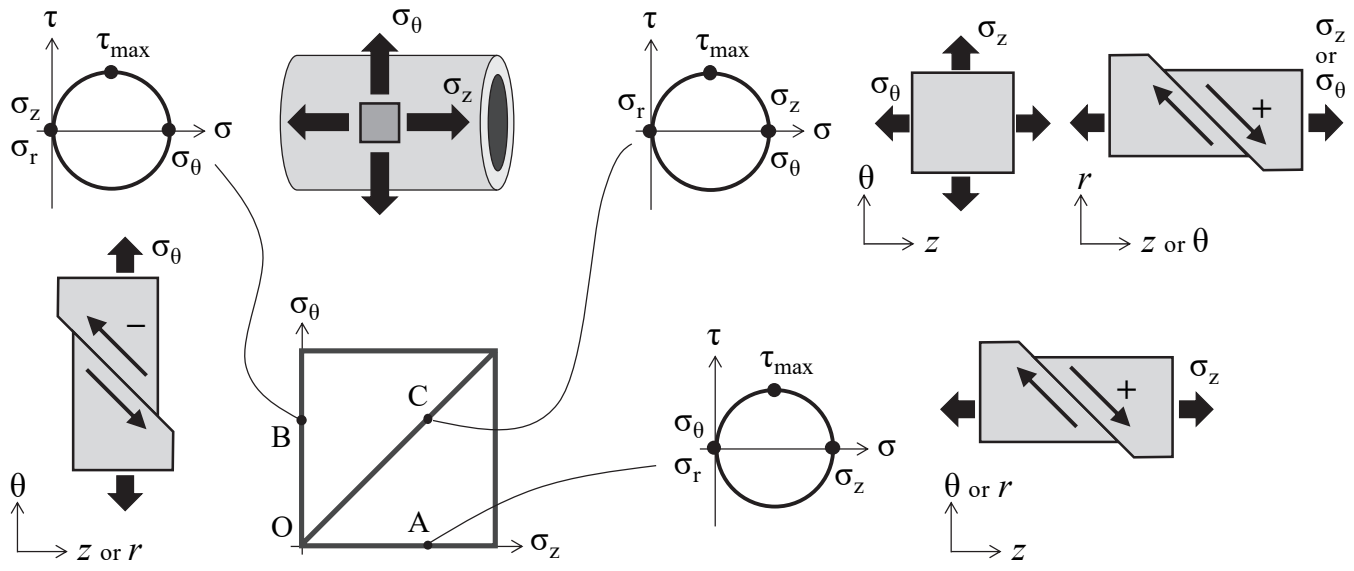

Figure 7: Maximum principal shear stress planes at each loading condition.

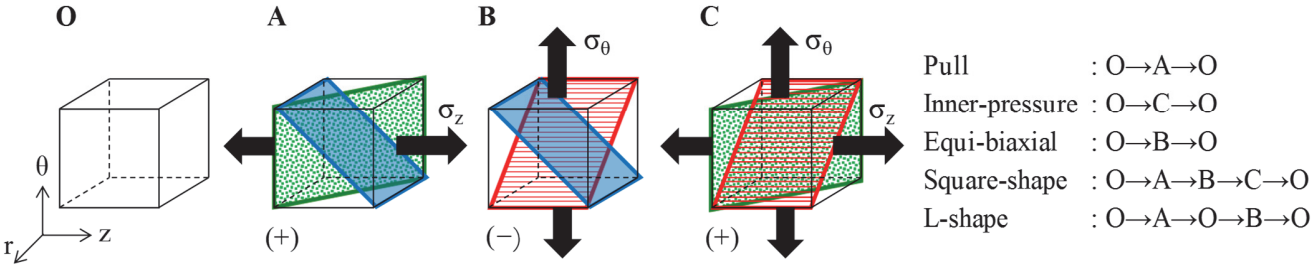

Figure 8: Schematic showing of slip planes at each loading condition.

Surface crack

Fig. 9 shows specimen surface and crack observations. Specimens in the Square-shape and the L-shape tests show barreling obviously which may be resulted from the larger possibility of slip activation related to the notable cyclic ratcheting deformation. In the crack observation, the length of all cracks observed are relative small size less than 4 mm. The tests were interrupted by oil leaking and the length of 4 mm is enough to stop the test. However, the size is too small to reach a through crack which is considered as the crack initiated from inside of the specimen.

To confirm the crack initiation and propagation behaviors, more detailed observations of crack on specimen and fracture surfaces are necessary, which are future works.

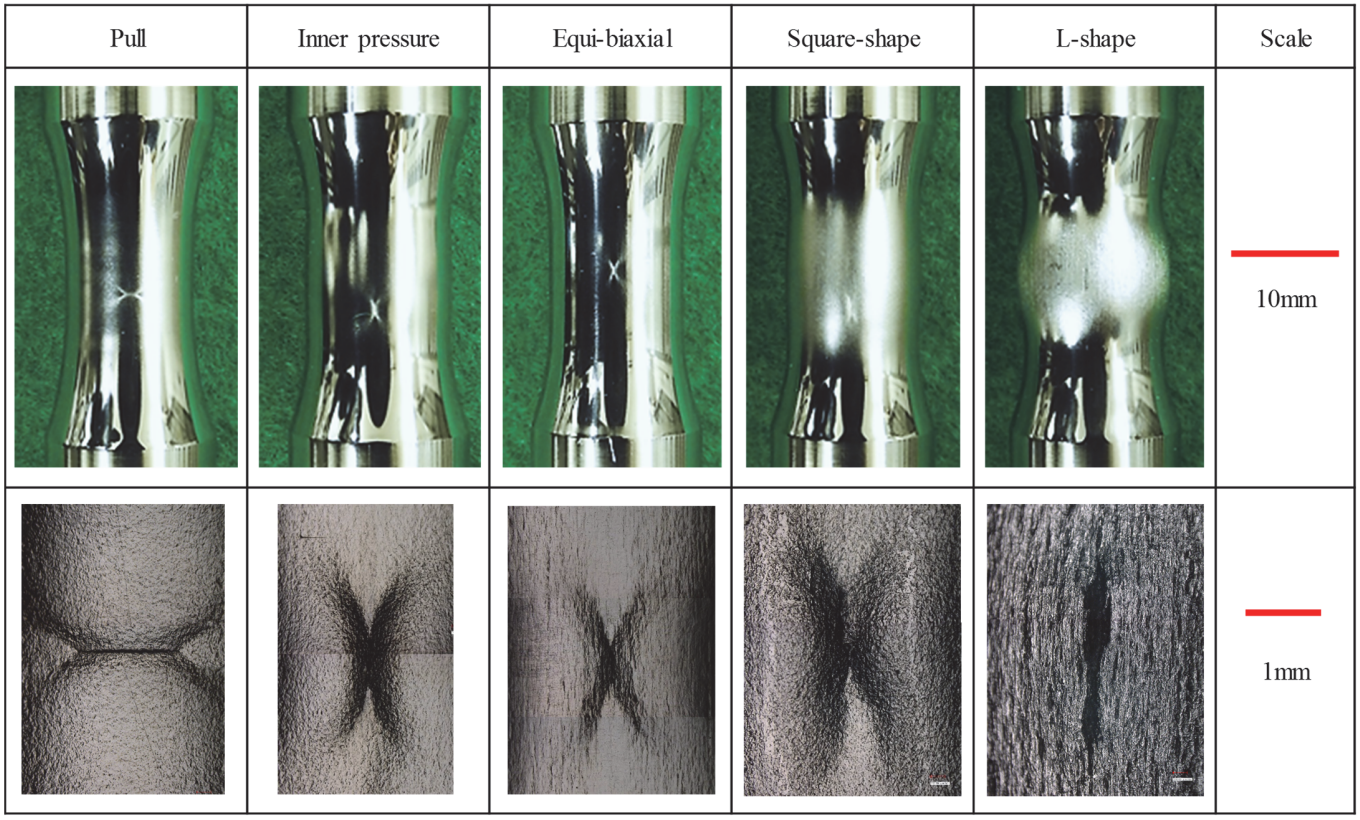

Figure 9: Specimen surface and crack observations.

CONCLUSIONS

Stress controlled multiaxial fatigue tests under wide ranged stress ratios were carried out using the newly developed fatigue testing machine which can apply push-pull loading and reversed torsion loading and inner pressure to the hollow cylinder specimen and the obtained results are shown as below;

1. Fatigue lives in the Pull, the Inner-pressure and the Equi-biaxial tests can be correlated by a unique line by the maximum value of Mises stress at the inner surface where cracks were initiated.
2. Fatigue lives in the L-shape and the Square-shape tests are reduced comparing with that in the Pull test, which are resulted from the larger cyclic ratcheting and barreling due to plastic deformation.

REFERENCES

[1] Nitta, A., Ogata, T., Kuwabara, K., The effect of axial-torsional straining phase on elevated-temperature biaxial low-cycle fatigue life in SUS 304 stainless steel, Journal of the Society of Materials Science, 36 (1989) 376−382.

[2] Doong, S.H., Socie, D.F., Robertson, I.M., Dislocation substructure and nonproportional hardening. Journal of Engineering Materials and Technology, 112(4) (1990) 456−464.

[3] Wang, C.H., Brown, M.W., A path-independent parameter for fatigue under proportional and non-proportional loading. Fatigue & Fracture of Engineering Materials & Structures, 16(12) (1993) 1285−1298.

[4] Itoh, T., Nakata, T., Sakane, M., Ohnami, M., Nonproportional low cycle fatigue of 6061 aluminum alloy under 14 strain paths. European Structural Integrity Society, 25 (1999) 41−54.

[5] Socie, D.F., Marquis, G.B., Multiaxial fatigue. Society of Automotive Engineers International, (2000) 129−339.

[6] Wiebesiek, J., Störzel, K., Bruder, T., Kaufmann, H., Multiaxial fatigue behaviour of laserbeam-welded thin steel and aluminium sheets under proportional and non-proportional combined loading, International Journal of Fatigue, 33(8) (2011) 992–1005.

[7] Bolchoun, A., Wiebesiek, J., Kaufmann, H., Sonsino, C.M., Application of stress-based multiaxial fatigue criteria for laserbeam-welded thin aluminium joints under proportional and non-proportional variable amplitude loadings, Theoretical and Applied Fracture Mechanics, 73 (2014) 9–16.

[8] Karolczuk, A., Analysis of revised fatigue life calculation algorithm under proportional and non-proportional loading with constant amplitude, International Journal of Fatigue, 88 (2016) 111–120.

[9] Fatemi, A., Socie, D.F., A critical plane approach to multiaxial fatigue damage including out-of-phase loading. Fatigue & Fracture of Engineering Materials & Structures, 11 (1988) 149−165.

[10] Carpinter, A., Brighenti, R., Macha, E., Spagnoli, A., Expected principal direction under multiaxial random loading. International Journal of Fatigue, 21 (1999) 89−96.

[11] Itoh, T., Miyazaki, T., A damage model for estimating low cycle fatigue lives under non-proportional multiaxial loading. Biaxial/Multiaxial Fatigue & Fracture, 31 (2003) 423−439.

[12] Itoh, T., Yang, T., Material dependence of multiaxial low cycle fatigue lives under non-proportional Loading. International Journal of Fatigue, 33(8) (2011) 1025−1031.

[13] Itoh, T., Sakane, M., Shimizu, Y., Definition of stress and strain ranges for multiaxial fatigue life evaluation under non-proportional loading, Journal of Society of Material Science, 62(2) (2013) 117−123.

[14] Itoh, T., Sakane, M., Morishita, T., Evaluation and visualization of multiaxial stress and strain states under non-proportional loading. Fracture and Structural Integrity, 33 (2015) 289−301.

[15] Paul, S.K., Prediction of non-proportional cyclic hardening and multiaxial fatigue life for FCC and BCC metals under constant amplitude of strain cycling, Materials Science and Engineering, 656(22) (2016) 111–119.

[16] Findley, W.N., Modified theory of fatigue failure under combined stress. Proceedings of the Society for Experimental Stress Analysis, 14 (1956) 35−46.

[17] Morishita, T., Itoh, T., Bao, Z., Multiaxial fatigue strength of type 316 stainless steel under push-pull, reversed torsion, cyclic inner and outer pressure loading, International Journal of Pressure Vessels and Piping, 140 (2016) 228−236.